Measurement of muon anti-neutrino oscillations with an accelerator-produced off-axis beam

K. Abe,[46] C. Andreopoulos,[44,26] M. Antonova,[21] S. Aoki,[23] A. Ariga,[1] S. Assylbekov,[7] D. Autiero,[28] M. Barbi,[39] G.J. Barker,[54] G. Barr,[35] P. Bartet-Friburg,[36] M. Batkiewicz,[12] F. Bay,[10] V. Berardi,[17] S. Berkman,[3] S. Bhadra,[58] A. Blondel,[11] S. Bolognesi,[5] S. Bordoni,[14] S.B. Boyd,[54] D. Brailsford,[25,16] A. Bravar,[11] C. Bronner,[22] M. Buizza Avanzini,[9] R.G. Calland,[22] S. Cao,[24] J. Caravaca Rodríguez,[14] S.L. Cartwright,[42] R. Castillo,[14] M.G. Catanesi,[17] A. Cervera,[15] D. Cherdack,[7] N. Chikuma,[45] G. Christodoulou,[26] A. Clifton,[7] J. Coleman,[26] G. Collazuol,[19] L. Cremonesi,[38] A. Dabrowska,[12] G. De Rosa,[18] T. Dealtry,[25] P.F. Denner,[54] S.R. Dennis,[54,44] C. Densham,[44] D. Dewhurst,[35] F. Di Lodovico,[38] S. Di Luise,[10] S. Dolan,[35] O. Drapier,[9] K. Duffy,[35] J. Dumarchez,[36] S. Dytman,[37] M. Dziewiecki,[53] S. Emery-Schrenk,[5] A. Ereditato,[1] T. Feusels,[3] A.J. Finch,[25] G.A. Fiorentini,[58] M. Friend,[13,*] Y. Fujii,[13,*] D. Fukuda,[33] Y. Fukuda,[30] A.P. Furmanski,[54] V. Galymov,[28] A. Garcia,[14] S.G. Giffin,[39] C. Giganti,[36] F. Gizzarelli,[5] M. Gonin,[9] N. Grant,[25] D.R. Hadley,[54] L. Haegel,[11] M.D. Haigh,[54] P. Hamilton,[16] D. Hansen,[37] T. Hara,[23] M. Hartz,[22,50] T. Hasegawa,[13,*] N.C. Hastings,[39] T. Hayashino,[24] Y. Hayato,[46,22] R.L. Helmer,[50] M. Hierholzer,[1] A. Hillairet,[51] A. Himmel,[8] T. Hiraki,[24] S. Hirota,[24] M. Hogan,[7] J. Holeczek,[43] S. Horikawa,[10] F. Hosomi,[45] K. Huang,[24] A.K. Ichikawa,[24] K. Ieki,[24] M. Ikeda,[46] J. Imber,[9] J. Insler,[27] R.A. Intonti,[17] T.J. Irvine,[47] T. Ishida,[13,*] T. Ishii,[13,*] E. Iwai,[13] K. Iwamoto,[40] A. Izmaylov,[15,21] A. Jacob,[35] B. Jamieson,[56] M. Jiang,[24] S. Johnson,[6] J.H. Jo,[32] P. Jonsson,[16] C.K. Jung,[32,†] M. Kabirnezhad,[31] A.C. Kaboth,[16,44] T. Kajita,[47,†] H. Kakuno,[48] J. Kameda,[46] D. Karlen,[51,50] I. Karpikov,[21] T. Katori,[38] E. Kearns,[2,22,†] M. Khabibullin,[21] A. Khotjantsev,[21] D. Kielczewska,[52] T. Kikawa,[24] H. Kim,[34] J. Kim,[3] S. King,[38] J. Kisiel,[43] A. Knight,[54] A. Knox,[25] T. Kobayashi,[13,*] L. Koch,[41] T. Koga,[45] A. Konaka,[50] K. Kondo,[24] A. Kopylov,[21] L.L. Kormos,[25] A. Korzenev,[11] Y. Koshio,[33,†] W. Kropp,[4] Y. Kudenko,[21,‡] R. Kurjata,[53] T. Kutter,[27] J. Lagoda,[31] I. Lamont,[25] E. Larkin,[54] M. Laveder,[19] M. Lawe,[25] M. Lazos,[26] T. Lindner,[50] Z.J. Liptak,[6] R.P. Litchfield,[54] X. Li,[32] A. Longhin,[19] J.P. Lopez,[6] L. Ludovici,[20] X. Lu,[35] L. Magaletti,[17] K. Mahn,[29] M. Malek,[42] S. Manly,[40] A.D. Marino,[6] J. Marteau,[28] J.F. Martin,[49] P. Martins,[38] S. Martynenko,[32] T. Maruyama,[13,*] V. Matveev,[21] K. Mavrokoridis,[26] W.Y. Ma,[16] E. Mazzucato,[5] M. McCarthy,[58] N. McCauley,[26] K.S. McFarland,[40] C. McGrew,[32] A. Mefodiev,[21] M. Mezzetto,[19] P. Mijakowski,[31] A. Minamino,[24] O. Mineev,[21] S. Mine,[4] A. Missert,[6] M. Miura,[46,†] S. Moriyama,[46,†] Th.A. Mueller,[9] S. Murphy,[10] J. Myslik,[51] T. Nakadaira,[13,*] M. Nakahata,[46,22] K.G. Nakamura,[24] K. Nakamura,[22,13,*] K.D. Nakamura,[24] S. Nakayama,[46,†] T. Nakaya,[24,22] K. Nakayoshi,[13,*] C. Nantais,[3] C. Nielsen,[3] M. Nirkko,[1] K. Nishikawa,[13,*] Y. Nishimura,[47] J. Nowak,[25] H.M. O'Keeffe,[25] R. Ohta,[13,*] K. Okumura,[47,22] T. Okusawa,[34] W. Oryszczak,[52] S.M. Oser,[3] T. Ovsyannikova,[21] R.A. Owen,[38] Y. Oyama,[13,*] V. Palladino,[18] J.L. Palomino,[32] V. Paolone,[37] N.D. Patel,[24] M. Pavin,[36] D. Payne,[26] J.D. Perkin,[42] Y. Petrov,[3] L. Pickard,[42] L. Pickering,[16] E.S. Pinzon Guerra,[58] C. Pistillo,[1] B. Popov,[36,§] M. Posiadala-Zezula,[52] J.-M. Poutissou,[50] R. Poutissou,[50] P. Przewlocki,[31] B. Quilain,[24] E. Radicioni,[17] P.N. Ratoff,[25] M. Ravonel,[11] M.A.M. Rayner,[11] A. Redij,[1] E. Reinherz-Aronis,[7] C. Riccio,[18] P. Rojas,[7] E. Rondio,[31] S. Roth,[41] A. Rubbia,[10] A. Rychter,[53] R. Sacco,[38] K. Sakashita,[13,*] F. Sánchez,[14] F. Sato,[13] E. Scantamburlo,[11] K. Scholberg,[8,†] S. Schoppmann,[41] J. Schwehr,[7] M. Scott,[50] Y. Seiya,[34] T. Sekiguchi,[13,*] H. Sekiya,[46,22,†] D. Sgalaberna,[10] R. Shah,[44,35] A. Shaikhiev,[21] F. Shaker,[56] D. Shaw,[25] M. Shiozawa,[46,22] T. Shirahige,[33] S. Short,[38] M. Smy,[4] J.T. Sobczyk,[57] M. Sorel,[15] L. Southwell,[25] P. Stamoulis,[15] J. Steinmann,[41] T. Stewart,[44] Y. Suda,[45] S. Suvorov,[21] A. Suzuki,[23] K. Suzuki,[24] S.Y. Suzuki,[13,*] Y. Suzuki,[22,22] R. Tacik,[39,50] M. Tada,[13,*] S. Takahashi,[24] A. Takeda,[46] Y. Takeuchi,[23,22] H.K. Tanaka,[46,†] H.A. Tanaka,[49,50,¶] D. Terhorst,[41] R. Terri,[38] T. Thakore,[27] L.F. Thompson,[42] S. Tobayama,[3] W. Toki,[7] T. Tomura,[46] C. Touramanis,[26] T. Tsukamoto,[13,*] M. Tzanov,[27] Y. Uchida,[16] A. Vacheret,[35] M. Vagins,[22,4] Z. Vallari,[32] G. Vasseur,[5] T. Wachala,[12] K. Wakamatsu,[34] C.W. Walter,[8,†] D. Wark,[44,35] W. Warzycha,[52] M.O. Wascko,[16] A. Weber,[44,35] R. Wendell,[46,†] R.J. Wilkes,[55] M.J. Wilking,[32] C. Wilkinson,[1] J.R. Wilson,[38] R.J. Wilson,[7] Y. Yamada,[13,*] K. Yamamoto,[34] M. Yamamoto,[24] C. Yanagisawa,[32,**] T. Yano,[23] S. Yen,[50] N. Yershov,[21] M. Yokoyama,[45,†] K. Yoshida,[24] T. Yuan,[6] M. Yu,[58] A. Zalewska,[12] J. Zalipska,[31] L. Zambelli,[13,*] K. Zaremba,[53] M. Ziembicki,[53] E.D. Zimmerman,[6] M. Zito,[5] and J. Żmuda[57]

(The T2K Collaboration)

[1] *University of Bern, Albert Einstein Center for Fundamental Physics, Laboratory for High Energy Physics (LHEP), Bern, Switzerland*

[2] *Boston University, Department of Physics, Boston, Massachusetts, U.S.A.*

[3] *University of British Columbia, Department of Physics and Astronomy, Vancouver, British Columbia, Canada*

[4] *University of California, Irvine, Department of Physics and Astronomy, Irvine, California, U.S.A.*

[5] *IRFU, CEA Saclay, Gif-sur-Yvette, France*
[6] *University of Colorado at Boulder, Department of Physics, Boulder, Colorado, U.S.A.*
[7] *Colorado State University, Department of Physics, Fort Collins, Colorado, U.S.A.*
[8] *Duke University, Department of Physics, Durham, North Carolina, U.S.A.*
[9] *Ecole Polytechnique, IN2P3-CNRS, Laboratoire Leprince-Ringuet, Palaiseau, France*
[10] *ETH Zurich, Institute for Particle Physics, Zurich, Switzerland*
[11] *University of Geneva, Section de Physique, DPNC, Geneva, Switzerland*
[12] *H. Niewodniczanski Institute of Nuclear Physics PAN, Cracow, Poland*
[13] *High Energy Accelerator Research Organization (KEK), Tsukuba, Ibaraki, Japan*
[14] *Institut de Fisica d'Altes Energies (IFAE), The Barcelona Institute of Science and Technology, Campus UAB, Bellaterra (Barcelona) Spain*
[15] *IFIC (CSIC & University of Valencia), Valencia, Spain*
[16] *Imperial College London, Department of Physics, London, United Kingdom*
[17] *INFN Sezione di Bari and Università e Politecnico di Bari, Dipartimento Interuniversitario di Fisica, Bari, Italy*
[18] *INFN Sezione di Napoli and Università di Napoli, Dipartimento di Fisica, Napoli, Italy*
[19] *INFN Sezione di Padova and Università di Padova, Dipartimento di Fisica, Padova, Italy*
[20] *INFN Sezione di Roma and Università di Roma "La Sapienza", Roma, Italy*
[21] *Institute for Nuclear Research of the Russian Academy of Sciences, Moscow, Russia*
[22] *Kavli Institute for the Physics and Mathematics of the Universe (WPI), The University of Tokyo Institutes for Advanced Study, University of Tokyo, Kashiwa, Chiba, Japan*
[23] *Kobe University, Kobe, Japan*
[24] *Kyoto University, Department of Physics, Kyoto, Japan*
[25] *Lancaster University, Physics Department, Lancaster, United Kingdom*
[26] *University of Liverpool, Department of Physics, Liverpool, United Kingdom*
[27] *Louisiana State University, Department of Physics and Astronomy, Baton Rouge, Louisiana, U.S.A.*
[28] *Université de Lyon, Université Claude Bernard Lyon 1, IPN Lyon (IN2P3), Villeurbanne, France*
[29] *Michigan State University, Department of Physics and Astronomy, East Lansing, Michigan, U.S.A.*
[30] *Miyagi University of Education, Department of Physics, Sendai, Japan*
[31] *National Centre for Nuclear Research, Warsaw, Poland*
[32] *State University of New York at Stony Brook, Department of Physics and Astronomy, Stony Brook, New York, U.S.A.*
[33] *Okayama University, Department of Physics, Okayama, Japan*
[34] *Osaka City University, Department of Physics, Osaka, Japan*
[35] *Oxford University, Department of Physics, Oxford, United Kingdom*
[36] *UPMC, Université Paris Diderot, CNRS/IN2P3, Laboratoire de Physique Nucléaire et de Hautes Energies (LPNHE), Paris, France*
[37] *University of Pittsburgh, Department of Physics and Astronomy, Pittsburgh, Pennsylvania, U.S.A.*
[38] *Queen Mary University of London, School of Physics and Astronomy, London, United Kingdom*
[39] *University of Regina, Department of Physics, Regina, Saskatchewan, Canada*
[40] *University of Rochester, Department of Physics and Astronomy, Rochester, New York, U.S.A.*
[41] *RWTH Aachen University, III. Physikalisches Institut, Aachen, Germany*
[42] *University of Sheffield, Department of Physics and Astronomy, Sheffield, United Kingdom*
[43] *University of Silesia, Institute of Physics, Katowice, Poland*
[44] *STFC, Rutherford Appleton Laboratory, Harwell Oxford, and Daresbury Laboratory, Warrington, United Kingdom*
[45] *University of Tokyo, Department of Physics, Tokyo, Japan*
[46] *University of Tokyo, Institute for Cosmic Ray Research, Kamioka Observatory, Kamioka, Japan*
[47] *University of Tokyo, Institute for Cosmic Ray Research, Research Center for Cosmic Neutrinos, Kashiwa, Japan*
[48] *Tokyo Metropolitan University, Department of Physics, Tokyo, Japan*
[49] *University of Toronto, Department of Physics, Toronto, Ontario, Canada*
[50] *TRIUMF, Vancouver, British Columbia, Canada*
[51] *University of Victoria, Department of Physics and Astronomy, Victoria, British Columbia, Canada*
[52] *University of Warsaw, Faculty of Physics, Warsaw, Poland*
[53] *Warsaw University of Technology, Institute of Radioelectronics, Warsaw, Poland*
[54] *University of Warwick, Department of Physics, Coventry, United Kingdom*
[55] *University of Washington, Department of Physics, Seattle, Washington, U.S.A.*
[56] *University of Winnipeg, Department of Physics, Winnipeg, Manitoba, Canada*
[57] *Wroclaw University, Faculty of Physics and Astronomy, Wroclaw, Poland*
[58] *York University, Department of Physics and Astronomy, Toronto, Ontario, Canada*

(Dated: December 9, 2015)

T2K reports its first measurements of the parameters governing the disappearance of $\overline{\nu}_\mu$ in an off-axis beam due to flavor change induced by neutrino oscillations. The quasi-monochromatic $\overline{\nu}_\mu$ beam, produced with a peak energy of 0.6 GeV at J-PARC, is observed at the far detector Super-Kamiokande, 295 km away, where the $\overline{\nu}_\mu$ survival probability is expected to be minimal. Using a dataset corresponding to 4.01×10^{20} protons on target, 34 fully contained μ-like events were observed.

The best-fit oscillation parameters are: $\sin^2(\overline{\theta}_{23}) = 0.45$ and $|\Delta\overline{m}^2_{32}| = 2.51 \times 10^{-3}$ eV^2 with 68% confidence intervals of 0.38 - 0.64 and 2.26 - 2.80 ($\times 10^{-3}$ eV^2) respectively. These world-leading results are in agreement with existing anti-neutrino parameter measurements and also with the ν_μ disappearance parameters measured by T2K.

PACS numbers: 14.60.Pq,14.60.Lm,11.30.Er,95.55.Vj

Introduction.—In the three-flavor framework, neutrino oscillation can be described by the unitary PMNS matrix, which is parameterized by three angles $\theta_{12}, \theta_{23}, \theta_{13}$ and a CP-violating phase δ_{CP} [1–3]. Given a neutrino propagation distance, L (km), and energy, E_ν (GeV), such that $L/E_\nu \sim O(1000)$, the survival probability for a muon neutrino propagating through vacuum can be approximated by:

$$P(\nu_\mu \to \nu_\mu) \simeq 1 - 4\cos^2(\theta_{13})\sin^2(\theta_{23})\times \\ [1 - \cos^2(\theta_{13})\sin^2(\theta_{23})]\sin^2(\frac{1.267\Delta m^2_{32}L}{E_\nu}), \quad (1)$$

where Δm^2_{32} (eV^2) is the neutrino mass squared splitting, defined as $m^2_3 - m^2_2$. In this model of neutrino oscillation, the disappearance probability in vacuum is identical for neutrinos and anti-neutrinos. The disappearance probabilities in matter can differ by as much as 0.1% for the T2K baseline and neutrino flux, but our dataset is not sensitive to this small effect. Observing a significant difference between the disappearance probabilities of neutrinos and anti-neutrinos would, therefore, be evidence for new physics [3]. Results from the MINOS [4] and Super-Kamiokande [5] collaborations indicate no significant difference between muon anti-neutrino oscillations and muon neutrino oscillations.

In this Letter we present the first measurement of $P(\overline{\nu}_\mu \to \overline{\nu}_\mu)$ by the T2K collaboration. This analysis allows the dominant anti-neutrino oscillation parameters for $\overline{\nu}_\mu$ disappearance to vary independently from those describing neutrino oscillations, *i.e.* $\theta_{23} \neq \overline{\theta}_{23}$ and $\Delta m^2_{32} \neq \Delta\overline{m}^2_{32}$, where the barred parameters refer to anti-neutrino oscillations. $\overline{\theta}_{13}$, $\overline{\theta}_{12}$ and $\Delta\overline{m}^2_{21}$ are assumed to be identical to their matter counterparts since our dataset cannot constrain them. This ensures that the expected background at the far detector is consistent with the current knowledge of neutrino oscillations, while allowing us to use the T2K anti-neutrino mode data to measure $\overline{\theta}_{23}$ and $\Delta\overline{m}^2_{32}$.

T2K experiment.—The T2K experiment [6] is composed of a neutrino beam line, a suite of near detectors, and the far detector, Super-Kamiokande (SK). Both the far detector and one of the near detectors are placed 2.5° off the neutrino beam axis and so observe a narrow-band beam [7]. This "off-axis" method reduces backgrounds from higher-energy neutrinos, producing a neutrino flux that peaks around 0.6 GeV, the energy at which the first minimum in the $\overline{\nu}_\mu$ survival probability is expected to occur at the T2K baseline.

The J-PARC main ring provides a 30 GeV proton beam which impinges upon a graphite target, producing pions and kaons. The target is held inside the first of three magnetic horns which focus charged particles into a 96-m-long decay volume, where they decay and produce neutrinos. The polarity of the horn current determines whether positive or negative mesons are focused, which in turn determines whether the neutrino beam is largely composed of muon neutrinos or muon anti-neutrinos. The decay volume ends in a beam dump followed by the muon monitor, which measures the neutrino beam direction on a bunch-by-bunch basis using muons from the meson decays.

The near detector complex [6] consists of the on-axis Interactive Neutrino GRID detector (INGRID) [8] and the off-axis detector (ND280), both 280 m downstream of the proton beam target. INGRID is a 7+7 array of iron/scintillator detectors, arranged in a "cross" configuration at the beam center. INGRID provides high-statistics monitoring of the neutrino beam intensity, direction, profile, and stability and has shown that the neutrino beam direction is controlled to 0.4 mrad. ND280 consists of a number of sub-detectors installed inside the refurbished UA1/NOMAD magnet, which provides a 0.2 T field. The near detector analysis described here uses the tracker region of ND280, which consists of three Time Projection Chambers (TPC1, 2, 3) [9] interleaved with two Fine-Grained Detectors (FGD1, 2) [10]. The FGDs are the neutrino target and track charged particles coming from the interaction vertex, whilst the TPCs perform 3D tracking and determine the charge, momentum, and energy loss of each charged particle traversing them. The observed energy loss is used for particle identification which, when combined with particle charge information, allows a precise separation and measurement of the $\overline{\nu}_\mu$ (right-sign) and ν_μ (wrong-sign) interactions in the anti-neutrino mode beam.

The far detector SK is a 50-kiloton (22.5-kiloton fiducial mass) water Cherenkov detector [11, 12] where the volume is divided into an outer detector (OD) with 1,885 outward-facing 20 cm diameter photomultiplier tubes and an inner detector (ID) with 11,129 inward-facing 50 cm diameter photomultiplier tubes. The events arriving at SK from the J-PARC beam spill are synchronized with a global positioning system with < 150 ns precision.

The results presented here are based on data taken in three periods: two where the beam operated in anti-neutrino mode, (1) June 2014 and (2) November 2014 – June 2015, and one in neutrino mode, (3) November

2010 – May 2013. The oscillation analysis uses periods (1) and (2), whilst the near detector analysis uses data from periods (1) and (3). This corresponds to an exposure of 4.01×10^{20} protons-on-target (POT) in anti-neutrino mode for the oscillation analysis, and an exposure of 0.43×10^{20} POT in anti-neutrino mode plus 5.82×10^{20} POT in neutrino mode for the near detector analysis.

Analysis strategy.—This analysis resembles that of Ref. [13], fitting samples of charged-current (CC) interactions at ND280 to produce a tuned prediction of the unoscillated anti-neutrino spectrum at the far detector, including its associated uncertainty. This analysis differs from Ref. [13] in that both ν_μ and $\overline{\nu}_\mu$ samples at ND280 are fit. This ensures that the neutrino interaction model is consistent between both neutrino and anti-neutrino beam mode datasets and provides a constraint on both the right-sign signal and the wrong-sign background in the anti-neutrino mode beam.

Flux simulation.—The nominal neutrino flux at ND280 and SK (without oscillation) is predicted by simulating the secondary beamline [14] using FLUKA2011 [15, 16] and GEANT3 with GCALOR [17, 18]. The simulated hadronic interactions are tuned to external hadron production data. The unoscillated neutrino flux prediction at SK is shown in Fig. 1 for each neutrino type and for both neutrino and anti-neutrino mode beams. At the peak energy of the T2K beam the ν_μ flux in the neutrino mode beam is 20% higher than the $\overline{\nu}_\mu$ flux in the anti-neutrino mode beam, due to the larger production cross section for π^+ compared to π^- in proton-carbon interactions. The ratio of the wrong-sign component (ν_μ in the $\overline{\nu}_\mu$ beam), mainly coming from forward-going high-energy pions, to the right-sign component ($\overline{\nu}_\mu$) at the peak energy is 3%. The largest sources of neutrino flux uncertainty are from beamline and hadron production modeling uncertainties, which are common to ND280 and SK. The new NA61/SHINE 2009 thin-target data [19] is included in the hadron production tuning for this analysis, reducing the total flux uncertainty from between 12-15% to 10% around 0.6 GeV.

Neutrino interaction simulation.—Neutrino interactions are modeled with the NEUT Monte Carlo event generator [20–23]. The generator uses the same model with common parameters to describe both ν and $\bar{\nu}$ interactions. In the case of CC quasi-elastic reactions (CCQE: $\nu_\mu + n \to \mu^- + p$ or $\overline{\nu}_\mu + p \to \mu^+ + n$) neutrino and anti-neutrino cross sections differ by the sign of the vector-axial interference term [24, 25]. At a neutrino energy of 0.6 GeV this makes the neutrino-oxygen CCQE cross section a factor of ~ 4 larger than that of anti-neutrinos.

To set the initial values and uncertainties of some parameters, such as the CCQE axial mass and the normalization of the multinucleon contribution, results from the MiniBooNE and MINERνA experiments [26–29] on CH_2 and CH targets are used. These parameters are then tuned by the near detector fit.

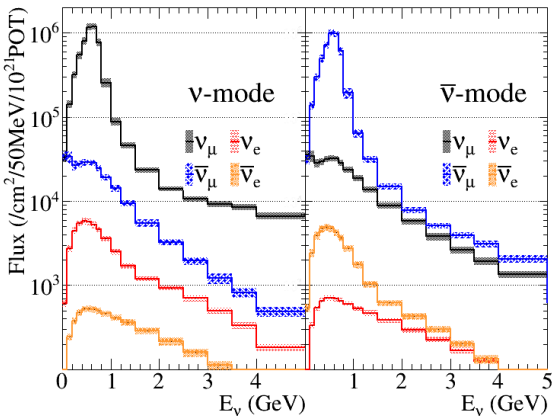

FIG. 1. The nominal unoscillated neutrino flux prediction at SK for each neutrino type in the neutrino mode beam (left) and anti-neutrino mode beam (right). The shaded boxes indicate the total systematic uncertainty on each energy bin.

TABLE I. Data and MC predicted event rates for the different ND280 samples before and after the fit. Errors indicate systematic uncertainties only.

Sample	Data	Prefit	Postfit
	ν beam mode		
ν_μ CC 0π	17362	15625 ± 1663	17248 ± 133
ν_μ CC $1\pi^+$	3988	4748 ± 686	4190 ± 60
ν_μ CC Other	4219	3772 ± 431	4079 ± 62
	$\bar{\nu}$ beam mode		
$\overline{\nu}_\mu$ CC 1-Track	435	387 ± 41	438 ± 13
$\overline{\nu}_\mu$ CC N-Tracks	136	128 ± 17	129 ± 5
ν_μ CC 1-Track	131	141 ± 15	147 ± 6
ν_μ CC N-Tracks	145	147 ± 17	144 ± 6

Near detector fit.— The seven samples used in the near detector fit are summarized in Table I. Muon neutrino induced CC interactions in the neutrino beam mode are found by requiring that the highest-momentum, negative-curvature track in an event starts within the upstream FGD (FGD1) fiducial volume (FV) and has an energy deposit in TPC2 consistent with a muon. Events with a TPC track that starts upstream of the start point of the muon candidate are rejected and the remaining ν_μ CC candidates are divided into three sub-samples according to the number of associated pions: ν_μ CC 0π, ν_μ CC $1\pi^+$, and ν_μ CC Other, dominated by CCQE, CC resonant pion production, and deep inelastic scattering interactions respectively [13]. For the anti-neutrino beam mode samples, the selection of $\overline{\nu}_\mu$ (ν_μ) CC interactions is similar to that used in the neutrino beam mode, except the positive (negative) track must be the highest momentum track in the event. The selected $\overline{\nu}_\mu$ (ν_μ) CC candidate events are divided into two sub-samples rather than

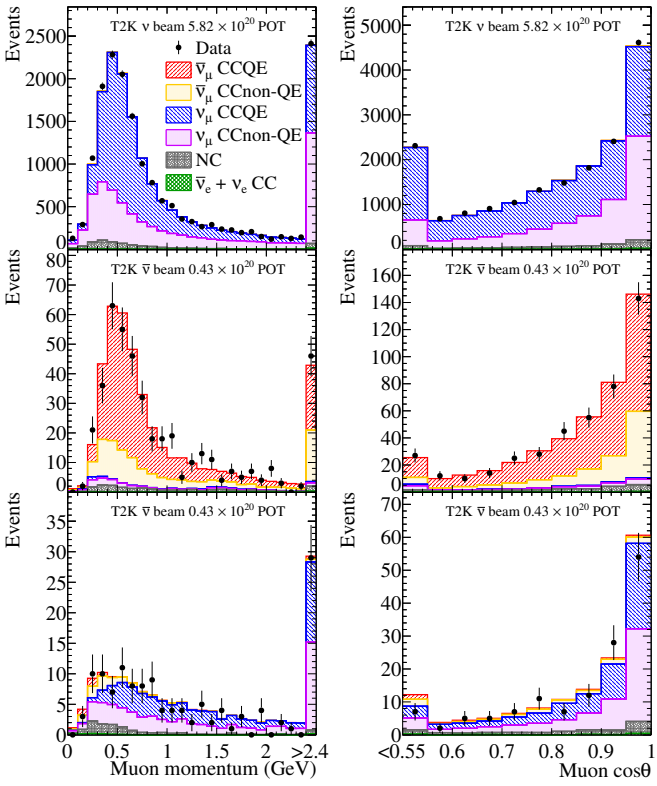

FIG. 2. The momentum (left) and angular (right) distributions of the muon candidates at ND280 from the ν_μ CC 0π (top), the $\overline{\nu}_\mu$ CC 1-Track (center) and the ν_μ CC 1-Track (bottom) samples. The data are superimposed on the post-fit MC prediction, separated by interaction mode.

three, due to the small amount of anti-neutrino mode data used in this analysis. These are defined by the number of reconstructed tracks crossing TPC2: $\overline{\nu}_\mu$ (ν_μ) CC 1-Track, dominated by CCQE interactions; and $\overline{\nu}_\mu$ (ν_μ) CC N-Tracks (N > 1), a mixture of resonant production and deep inelastic scattering.

The fit uses a binned likelihood, with the samples binned according to the muon momentum and angle (θ) relative to the central axis of the detector, roughly 1.7° away from the incident (anti-)neutrino direction. Figure 2 shows the 1D projections of these distributions for the ν_μ CC 0π, the $\overline{\nu}_\mu$ CC 1-Track and the ν_μ CC 1-Track samples in both data and fitted MC. The p-value of the data fit likelihood ratio was found to be 0.05, indicating acceptable agreement between the ND280 data and the MC model. The fit gives estimates for 25 anti-neutrino beam flux parameters at SK, 12 cross-section parameters (including 4 specific to oxygen) and their covariance. There are also additional parameters to control pion final state interactions (FSI) and reinteractions within the detector, which are independent for ND280 and SK.

To decouple the properties of the carbon target at ND280 from those of the oxygen target at SK, separate Fermi momentum, binding energy, multinucleon event normalization and CC coherent pion production normalization parameters are introduced for interactions on oxygen. Since oxygen comprises only 3.6% by mass of the FGD1 target, this near detector analysis is insensitive to these parameters. A conservative (100% uncertainty) ansatz is adopted for the normalization of multinucleon ejection oxygen events, giving a 9.5% uncertainty on the number of events at SK. For the parameters that ND280 can constrain, the fit reduces their effect on the uncertainty on the expected number of events at SK from 9.2% to 3.4%.

TABLE II. The number of events observed at the far detector in the anti-neutrino beam mode data after applying each selection cut. MC expected events are calculated assuming oscillations with $\sin^2(\theta_{23}) = \sin^2(\overline{\theta}_{23}) = 0.5$, $|\Delta m^2_{32}| = |\Delta \overline{m}^2_{32}| = 2.4 \times 10^{-3}$ eV^2, and $\sin^2(\theta_{13}) = \sin^2(\overline{\theta}_{13}) = 0.0257$. The "$\overline{\nu}_e$+$\nu_e$ +NC" column includes the NC interactions of all the (anti-)neutrino flavors. Efficiency numbers are calculated with respect to the number of MC events generated in the fiducial volume (FV interaction).

	Data	Total MC	CCQE $\overline{\nu}_\mu$	CCQE ν_μ	CCnonQE $\overline{\nu}_\mu$	CCnonQE ν_μ	$\overline{\nu}_e$+ν_e +NC
FV interaction	n/a	186.7	17.8	11.4	20.0	36.5	101
FCFV	90	99.7	14.4	8.6	15.1	26.6	35.1
Single ring	50	52.2	14.0	7.7	8.1	8.7	13.8
μ-like	40	39.4	13.8	7.6	7.8	8.0	2.2
$P_\mu > 0.2$ GeV	40	39.3	13.8	7.6	7.8	8.0	2.2
$N_{\text{decay-e}} < 2$	34	36.1	13.7	7.5	7.3	5.6	2.1
Efficiency (%)			77.1	65.7	36.6	15.3	2.0

Far detector selection.—At the far detector, fully contained fiducial volume (FCFV) events are selected by requiring no hit clusters in the OD, that the reconstructed interaction vertex is more than 2 m away from the ID wall, and that the visible energy in the event, defined as the energy of an electromagnetic shower producing a given amount of Cherenkov light, is larger than 30 MeV.

To enhance the $\overline{\nu}_\mu$ CCQE purity of the sample, selected events must have a single, μ-like Cherenkov ring, no more than one decay electron, and a muon momentum greater than 0.2 GeV [30]. The number of data and MC events passing each selection criterion are shown in Table II and the reconstructed energy spectrum of the 34 selected events is plotted in Fig. 3. The reconstructed neutrino energy is calculated using the muon momentum and production angle, under the assumption that a CCQE interaction occurred on a nucleon at rest. The selection efficiency for $\overline{\nu}_\mu$ CCQE is estimated to be 77% whilst backgrounds from neutral-current (NC), ν_e, and $\overline{\nu}_e$ interactions are reduced by a factor of 50. The systematic uncertainties in the detector response are evaluated using atmospheric neutrinos, cosmic-ray muons, and their decay electrons [13].

Oscillation fit.—The oscillation parameters $\sin^2(\overline{\theta}_{23})$

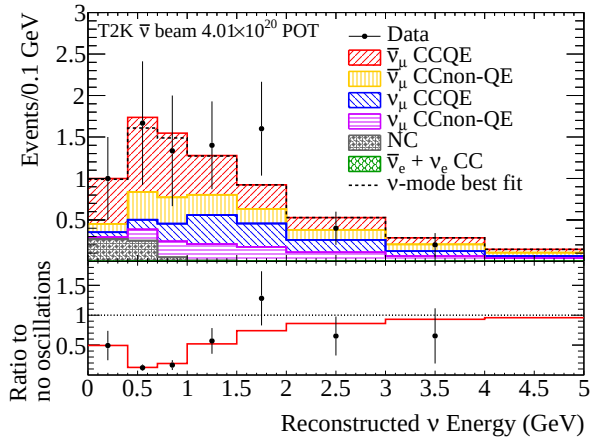

FIG. 3. Top: The reconstructed energy distribution of the 34 far detector $\overline{\nu}_\mu$ candidates and the best fit prediction, separated by interaction mode. This is compared to the predicted spectrum assuming the anti-neutrino oscillation parameters are identical to the neutrino parameters measured by T2K [13]. Bottom: The observed data and $\overline{\nu}_\mu$-mode best fit prediction as a ratio to the unoscillated prediction.

TABLE III. Oscillation parameters used for the fit. The parameters $\sin^2(\overline{\theta}_{23})$ and $\Delta\overline{m}^2_{32}$ were allowed to fit in the ranges given. All other parameters were fixed to the values shown, taken from previous T2K fits [13] and the Particle Data Group review [33].

Parameter	ν	$\overline{\nu}$
$\sin^2(\theta_{23})$	0.527	fit 0 – 1
Δm^2_{32} (10^{-3} eV^2)	2.51	fit 0 – 20
$\sin^2(\theta_{13})$	0.0248	
$\sin^2(\theta_{12})$	0.304	
Δm^2_{21} (10^{-5} eV^2)	7.53	
δ_{CP} (rad)	-1.55	

and $\Delta\overline{m}^2_{32}$ are estimated using a maximum likelihood fit to the measured reconstructed energy spectrum in the far detector. All other oscillation parameters are fixed as shown in Table III. Oscillation probabilities are calculated using the full three-flavor oscillation framework [31], assuming the normal mass hierarchy ($\Delta m^2_{32} > 0$). Matter effects are included with an Earth density of $\rho = 2.6$ g/cm^3 [32].

Confidence regions are constructed for the oscillation parameters using the constant $\Delta\chi^2$ method [33]. A marginal likelihood is used for this, integrating over the nuisance parameters $\mathbf{f}$ with prior probability functions $\pi(\mathbf{f})$ to find the likelihood as a function of only the relevant oscillation parameters $\mathbf{o}$:

$$\mathcal{L}(\mathbf{o}) = \int \prod_{i}^{\text{Ebins}} \mathcal{L}_i(\mathbf{o}, \mathbf{f}) \times \pi(\mathbf{f})\, d\mathbf{f}, \qquad (2)$$

where Ebins denotes the number of reconstructed neutrino energy bins.

TABLE IV. Percentage change in the number of 1-ring μ-like events before the oscillation fit from 1σ systematic parameter variations, assuming the oscillation parameters listed in Table III and that the anti-neutrino and neutrino oscillation parameters are identical.

Source of uncertainty (number of parameters)	$\delta n^{\text{exp}}_{\text{SK}}/n^{\text{exp}}_{\text{SK}}$
ND280-unconstrained cross section (6)	10.0%
Flux and ND280-constrained cross section (31)	3.4%
Super-Kamiokande detector systematics (6)	3.8%
Pion FSI and reinteractions (6)	2.1%
Total (49)	11.6%

We define $\Delta\chi^2 = -2\ln(\mathcal{L}(\mathbf{o})/\max(\mathcal{L}))$ as the ratio of the marginal likelihood at a point $\mathbf{o}$ in the $\sin^2(\overline{\theta}_{23})$ – $\Delta\overline{m}^2_{32}$ oscillation parameter space and the maximum marginal likelihood. The confidence region is then defined as the area of the oscillation parameter space for which $\Delta\chi^2$ is less than a standard critical value.

Table IV summarizes the fractional error on the expected number of SK events from a 1σ variation of the flux, cross-section, and far detector systematic parameters. Although the fractional error on the expected number of events due to systematic errors is large, the effect of systematic parameters on the confidence regions found in this fit is negligible due to the limited data statistics. The impact of fixing the values of $\sin^2(\theta_{23})$ and Δm^2_{32} in the fit is also negligible.

The observed $\overline{\nu}_\mu$ reconstructed energy spectrum from the anti-neutrino beam mode data is shown in the upper plot of Fig. 3, overlaid with the best fit spectrum assuming normal hierarchy, separated by interaction mode. The lower plot in Fig. 3 is the ratio of data to the expected, unoscillated spectrum.

The best fit values obtained are $\sin^2(\overline{\theta}_{23}) = 0.45$ and $|\Delta\overline{m}^2_{32}| = 2.51 \times 10^{-3}$eV^2, with 68% confidence intervals of 0.38 – 0.64 and 2.26 – 2.80 ($\times 10^{-3}$ eV^2) respectively. A goodness-of-fit test was performed by comparing this fit to an ensemble of toy experiments, giving a p-value of 0.38.

The fit results are shown in Fig. 4 as 68% and 90% confidence regions in the $\sin^2(\overline{\theta}_{23})$ – $\Delta\overline{m}^2_{32}$ plane. The 90% confidence regions from the T2K neutrino beam mode joint disappearance and appearance fit [13], the SK fit to $\overline{\nu}_\mu$ in atmospheric neutrino data [5], and the MINOS fit to $\overline{\nu}_\mu$ beam and atmospheric data [4] are also shown for comparison. A second, fully Bayesian, analysis was also performed, producing a credible region matching the confidence regions presented above.

Conclusions.—We report the first study of $\overline{\nu}_\mu$ disappearance using an off-axis beam and present measurements of $\sin^2(\overline{\theta}_{23}) = 0.45$ and $\Delta\overline{m}^2_{32} = 2.51 \times 10^{-3}$ eV^2. These results are consistent with the values of $\sin^2(\theta_{23})$ and Δm^2_{32} observed previously by T2K [13], providing

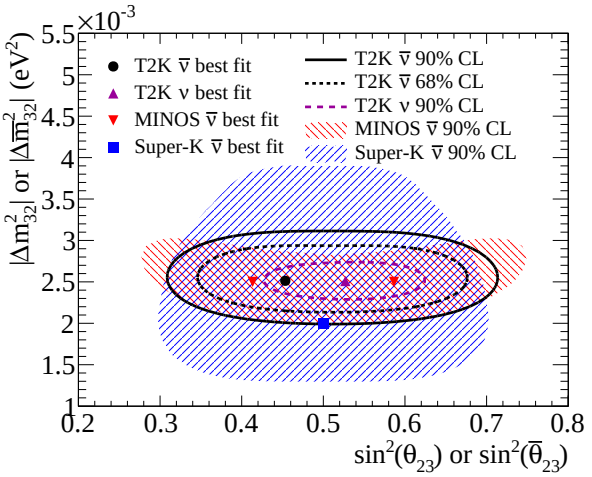

FIG. 4. The 68% and 90% confidence regions for $\sin^2(\bar{\theta}_{23})$ and $|\Delta\overline{m}^2_{32}|$ assuming normal hierarchy. T2K ν [13], SK $\overline{\nu}$ [5] and MINOS $\overline{\nu}$ [4] 90% confidence regions are also shown.

no indication of new physics, and are also in good agreement with similar measurements from MINOS [4] and SK [5]. The results presented here, with the first T2K anti-neutrino dataset, are competitive with those from both MINOS and SK, demonstrating the effectiveness of the off-axis beam technique.

We thank the J-PARC staff for superb accelerator performance and the CERN NA61 collaboration for providing valuable particle production data. We acknowledge the support of MEXT, Japan; NSERC (grant SAPPJ-2014-00031), NRC and CFI, Canada; CEA and CNRS/IN2P3, France; DFG, Germany; INFN, Italy; National Science Centre (NCN), Poland; RSF, RFBR and MES, Russia; MINECO and ERDF funds, Spain; SNSF and SERI, Switzerland; STFC, UK; and DOE, USA. We also thank CERN for the UA1/NOMAD magnet, DESY for the HERA-B magnet mover system, NII for SINET4, the WestGrid and SciNet consortia in Compute Canada, GridPP and the Emerald High Performance Computing facility, UK. In addition participation of individual researchers and institutions has been further supported by funds from: ERC (FP7), H2020 RISE-GA644294-JENNIFER, EU; JSPS, Japan; Royal Society, UK; DOE Early Career program, USA.

* also at J-PARC, Tokai, Japan
† affiliated member at Kavli IPMU (WPI), the University of Tokyo, Japan
‡ also at National Research Nuclear University "MEPhI" and Moscow Institute of Physics and Technology, Moscow, Russia
§ also at JINR, Dubna, Russia
¶ also at Institute of Particle Physics, Canada
** also at BMCC/CUNY, Science Department, New York, New York, U.S.A.

[1] Z. Maki, M. Nakagawa, and S. Sakata, Prog. Theor. Phys. **28**, 870 (1962).
[2] B. Pontecorvo, Sov. Phys. JETP **26**, 984 (1968).
[3] K. Nakamura, S. T. Petcov, et al. (Particle Data Group), Phys. Rev. D **86**, 010001 (2012), see section 13. NEUTRINO MASS, MIXING, AND OSCILLATIONS.
[4] P. Adamson et al. (MINOS Collaboration), Phys. Rev. Lett. **108**, 191801 (2012).
[5] K. Abe et al. (Super-Kamiokande Collaboration), Phys. Rev. Lett. **107**, 241801 (2011).
[6] K. Abe et al. (T2K Collaboration), Nucl. Instrum. Methods **A659**, 106 (2011).
[7] D. Beavis, A. Carroll, I. Chiang, et al. (E889 Collaboration), Physics Design Report **BNL 52459** (1995).
[8] K. Abe et al. (T2K Collaboration), Nucl. Instrum. Methods **A694**, 211 (2012).
[9] N. Abgrall et al. (T2K ND280 TPC Collaboration), Nucl. Instrum. Methods **A637**, 25 (2011).
[10] P. Amaudruz et al. (T2K ND280 FGD Collaboration), Nucl. Instrum. Methods **A696**, 1 (2012).
[11] S. Fukuda et al. (Super-Kamiokande Collaboration), Nucl. Instrum. Methods **A501**, 418 (2003).
[12] K. Abe et al. (Super-Kamiokande Collaboration), Nucl. Instrum. Methods **A737**, 253 (2014).
[13] K. Abe et al. (T2K Collaboration), Phys. Rev. **D91**, 072010 (2015).
[14] K. Abe et al. (T2K Collaboration), Phys. Rev. **D87**, 012001 (2013), [Addendum: Phys. Rev.D87,no.1,019902(2013)].
[15] A. Ferrari, P. R. Sala, A. Fasso, and J. Ranft, Report No. CERN-2005-010 and SLAC-R-773 and INFN-TC-05-11 (2005).
[16] T. T. Böhlen et al., Nuclear Data Sheets **120**, 211 (2014).
[17] R. Brun, F. Carminati, and S. Giani, Report No. CERN-W5013 (1994).
[18] C. Zeitnitz and T. A. Gabriel, *In Proc. of International Conference on Calorimetry in High Energy Physics, Tallahassee, FL, USA, February 1993.*
[19] N. Abgrall et al. (NA61/SHINE), (2015), arXiv:1510.02703 [hep-ex].
[20] Y. Hayato, Acta Phys. Polon. **B40**, 2477 (2009), version 5.3.2 of NEUT library is used that includes (i) the multinucleon ejection model of Nieves *et al.* [21] and (ii) nuclear long range correlations for CCQE interactions, treated in the random phase approximation [22].
[21] J. Nieves, I. Ruiz Simo, and M. J. Vicente Vacas, Phys. Rev. C **83**, 045501 (2011).
[22] J. Nieves, J. E. Amaro, and M. Valverde, Phys. Rev. C **70**, 055503 (2004), [Erratum-ibid. C **72** (2005) 019902].
[23] C. Wilkinson, *In Proc. of 16th International Workshop on Neutrino Factories and Future Neutrino Beam Facilities (NUFACT 2014), Glasgow, Scotland, UK, August 2014* .
[24] C. H. Llewellyn Smith, Phys. Rept. **3**, 261 (1972).
[25] M. Jacob, Gauge Theories and Neutrino Physics (Elsevier Science Ltd, North-holland/amsterdam, 1978).
[26] A. A. Aguilar-Arevalo *et al.* [MiniBooNE Collaboration], Phys. Rev. D **81**, 092005 (2010).
[27] A. A. Aguilar-Arevalo et al. (MiniBooNE), Phys. Rev. **D88**, 032001 (2013).
[28] G. Fiorentini et al. (MINERvA Collaboration), Phys. Rev. Lett. **111**, 022502 (2013).

[29] L. Fields et al. (MINERvA Collaboration), Phys. Rev. Lett. **111**, 022501 (2013).
[30] K. Abe et al. (T2K Collaboration), Phys. Rev. D **91**, 072010 (2015).
[31] V. Barger, K. Whisnant, S. Pakvasa, and R. J. N. Phillips, Phys. Rev. D **22**, 2718 (1980).
[32] K. Hagiwara, N. Okamura, and K. Senda, Journal of High Energy Physics **2011**, 82 (2011).
[33] K. A. Olive et al. (Particle Data Group), Chin. Phys. **C38**, 090001 (2014).